T cell-depleting nanoparticles ameliorate bone loss by reducing activated T cells and regulating the Treg/Th17 balance

Xiaoshan Yang [a,b,1], Fuxing Zhou [c,1], Pingyun Yuan [d,1], Geng Dou [a], Xuemei Liu [a], Siying Liu [a], Xiangdong Wang [a], Ronghua Jin [a], Yan Dong [a], Jun Zhou [a], Yajie Lv [e], Zhihong Deng [a], Shiyu Liu [a,****], Xin Chen [d,***], Ying Han [b,**], Yan Jin [a,*]

[a] State Key Laboratory of Military Stomatology & National Clinical Research Center for Oral Diseases & Shaanxi International Joint Research Center for Oral Diseases, Center for Tissue Engineering, School of Stomatology, Fourth Military Medical University, Xi'an, Shaanxi, 710032, China
[b] Xijing Hospital of Digestive Diseases & State Key Laboratory of Cancer Biology, Fourth Military Medical University, Xi'an, Shaanxi, 710032, China
[c] Department of Gynecology and Obstetrics, Xijing Hospital, Fourth Military Medical University, Xi'an, Shaanxi, 710032, China
[d] School of Chemical Engineering and Technology, Shaanxi Key Laboratory of Energy Chemical Process Intensification, Institute of Polymer Science in Chemical Engineering, Xi'an Jiao Tong University, Xi'an, Shaanxi, 710049, China
[e] Department of Dermatology, Tangdu Hospital, Fourth Military Medical University, Xi'an, Shaanxi, 710038, China

ARTICLE INFO

ABSTRACT

Estrogen deficiency is one of the most frequent causes of osteoporosis in postmenopausal women. Under chronic inflammatory conditions caused by estrogen deficiency, activated T cells contribute to elevated levels of proinflammatory cytokines, impaired osteogenic differentiation capabilities of bone marrow mesenchymal stem cells (BMMSCs), and disturbed regulatory T cell (Treg)/Th17 cell balance. However, therapeutic strategies that re-establish immune homeostasis in this disorder have not been well developed. Here, we produced T cell-depleting nanoparticles (TDNs) that ameliorated the osteopenia phenotype and rescued the osteogenic deficiency of BMMSCs in ovariectomized (OVX) mice. TDNs consist of monocyte chemotactic protein-1 (MCP-1)-encapsulated mesoporous silica nanoparticles as the core and Fas-ligand (FasL) as the corona. We showed that the delicate design of the TDNs enables rapid release of MCP-1 to recruit activated T cells and then induces their apoptosis through the conjugated FasL both *in vitro* and *in vivo*. Apoptotic signals recognized by macrophages help skew the Treg/Th17 cell balance and create an immune tolerant state, further attenuating the osteogenic deficiency of BMMSCs and the osteopenia phenotype. Mechanistically, we found that the therapeutic effects of TDNs were partially mediated by apoptotic T cell-derived extracellular vesicles (ApoEVs), which promoted macrophage transformation towards the M2 phenotype. These findings demonstrate that TDNs may represent a promising strategy for treating osteoporosis and other immune disorders.

1. Introduction

Estrogen plays a fundamental role in bone homeostasis and its deficiency is one of the most frequent causes of osteoporosis in postmenopausal women [1]. Increasing evidence indicates that bone and immune cells are closely connected [2]. The effects of estrogen on bone are mediated to a large extent by its action on immune cells [3]. Under conditions of estrogen deficiency, T cells are overactivated, and they secrete pro-osteoclastogenic factors, including interleukin 17 (IL-17), interleukin 6 (IL-6), tumor necrosis factor α (TNF-α) and receptor activator of NF-kB ligand (RANKL) to promote osteoclast formation and accelerate bone resorption, resulting in bone loss [4,5]. These findings

---

suggest that activated T cells play a pivotal role in the mechanism of estrogen deficiency-associated bone loss.

It has also been well described that under chronic inflammatory conditions caused by estrogen deficiency, T cell subsets are altered and the regulatory T cell (Tregs)/Th17 cell balance is disrupted [6,7]. Tregs are immunosuppressive cells that can inhibit osteoclast differentiation, while Th17 cells represent a proinflammatory subset that can contribute to osteoclast differentiation [8]. However, Tregs may lose their immunosuppressive function and convert to Th17 cells under osteoporotic pathological conditions [9]. Therefore, it would be reasonable to eliminate excessive activated T cells and remodel immune homeostasis under estrogen deficiency conditions.

Many FDA-approved therapies for osteoporosis are antiresorptive drugs that primarily act by reducing osteoclast activity, such as bisphosphonates and denosumab (a monoclonal antibody that neutralizes RANKL) [10]. However, these treatments may impair intrinsic repair mechanisms and increase the risk of atypical femur fractures [10,11]. Although studies have shown that activated T cells are key mediators of ovariectomy (OVX)-induced bone loss, there is little research on the effects of T cell depletion treatment. In recent decades, nanoparticles have been widely used as nano-based drug delivery systems to achieve accurate molecule delivery [12,13]. Based on their unique intrinsic properties, such as large surface area and pore volume, mesoporous silica nanoparticles (MSNs), have significant advantages over traditional drug nanocarriers [14,15].

In the present study, we synthesized T-cell depleting MSNs (TDNs). MCP-1, a key mediator in inflammation that induces T cell migration to sites of inflammation [16], was encapsulated in the TDNs as a core to recruit T cells. In addition, Fas, a member of the cell death receptor family, is increasingly expressed in activated T cells and its binding with FasL results in programmed cell death [17]. Inspired by this, we conjugated FasL onto the surface of TDNs to trigger apoptosis of activated T cells. This delicate design enabled TDNs to eliminate excessive activated T cells to help re-establish an immune tolerant microenvironment to ameliorate osteoporosis (Scheme 1).

2. Materials and methods

2.1. Materials

(3-Aminopropyl) trimethoxysilane, tetraethyl orthosilicate, N-cetyltrimethylammonium bromide (CTAB), ammonium hydroxide and 1,3,5-trimethylbenzene were purchased from Sigma-Aldrich. Double epoxy-modified polyethylene (EO-PEG-EO) was obtained from Energy Chemical. Hydrochloric acid, chloroform and ethanol were purchased from Security Chemical.

### 2.2. Preparation of TDNs

2.2.1. MSNs

MSNs were prepared according to our previous work [18]. CTAB (1.12 g) was added to deionized water (1000 ml) with a pH of 11 at 50 °C, followed by addition of tetraethyl orthosilicate (5.8 ml) under vigorous stirring and further reaction for 2 h. After ageing overnight, the mixture was centrifuged and washed with deionized water and absolute ethanol. The obtained products were dispersed in anhydrous ethanol and sonicated to obtain a uniform suspension. Then, a 1:1 mixture (20 ml, v/v) of water and 1,3,5-trimethylbenzene were added to the suspension and placed in an autoclave. The autoclave was set in a stove at a temperature of 140 °C for 4 days. Subsequently, the products were washed with absolute ethanol and deionized water five times respectively. The resulting silicon nanoparticles were dispersed in acidic ethanol and followed by reflux for 36 h at 70 °C. Finally, the mixture was centrifuged, washed three times with ethanol and dried under a vacuum to obtain mesoporous silica nanoparticles (MSNs) with large pores.

2.2.2. MSNs-NH₂

The as-prepared MSNs (0.2 g) were dispersed in 10 ml of ethanol and sonicated for 20 min to obtain uniform dispersion. Then (3-aminopropyl) trimethoxysilane (0.1 ml) was added to the suspension. The mixture was stirred for 12 h at room temperature for amino functionalization. Next, the solution was centrifuged, washed three times with ethanol and dried in a vacuum oven at 40 °C overnight.

2.2.3. MSNs-PEG-EO

MSNs-PEG-EO were synthesized by a ring-opening reaction between amino groups from MSNs-NH₂ and epoxy groups from polyethylene glycol diglycidyl ether (EO-PEG-EO). To perform this reaction, as-synthesized MSNs-NH₂ (0.1 g) and commoditized EO-PEG-EO (0.1 g) were dispersed in distilled water (20 ml), followed by sonication for 15 min to acquire a homogeneous dispersion. Then the mixture was stirred overnight at room temperature. After that, the suspension was centrifuged, washed three times with distilled water and freeze dried to obtain MSNs-PEG-EO.
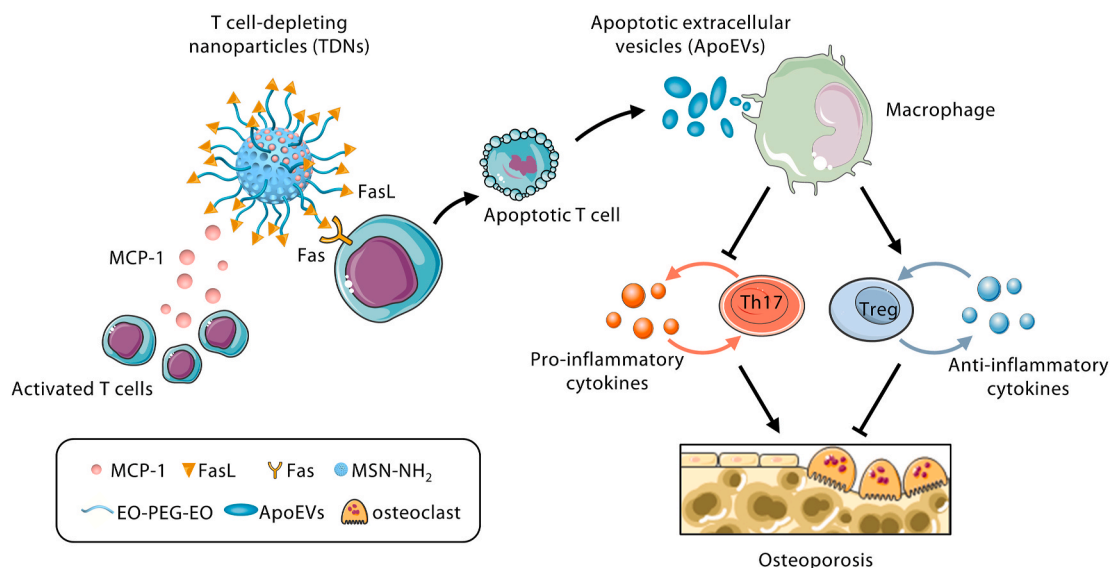
Scheme 1. Schematic illustration of TDNs and their therapeutic effects on osteoporosis through induction of T cell apoptosis and regulation of the Tregs/Th17 balance.

2.2.4. FasL-conjugated and MCP-1-loaded MSNs-PEG-EO

The as-synthesized MSNs-PEG-EO were dispersed in PBS and sonicated for 10 min to achieve a uniform dispersion, followed by the addition of FasL (0.2 wt%, each milligram of TDNs contains 2 μg of FasL). After stirring at 4 °C overnight, the mixture was centrifuged and washed with deionized water three times. The obtained precipitate was redistributed in PBS, and MCP-1 was added. After incubation at 4 °C for 24 h, TDNs were acquired by centrifugation, washing with deionized water, and freezing lyophilization. The structure and abbreviations of the various nanoparticles with specific molecules described in this paper are shown in Table 1.

2.3. Mice

Eight-week-old female C57BL/6 mice were purchased from the Animal Center of Fourth Military Medical University (Xi'an, China). Mice were housed on a 12 h light/12 h dark cycle with ad libitum access to food pellets and tap water. All procedures involving animals were approved by the Animal Use and Care Committee of the Fourth Military Medical University.

2.4. Splenic T cell culture and activation

A mouse splenic T cell suspension was collected by homogenizing the spleens of mice. ACK lysis buffer (Beyotime, C3702) was used to remove red blood cells. The cell suspension was cultured in RPMI 1640 medium (Gibco) supplemented with 10% fetal bovine serum (FBS), 50 mM 2-mercaptoethanol, 2 mM L-glutamine (Sigma-Aldrich), and 1% penicillin/streptomycin (Invitrogen). For T cell activation, the plate was coated with anti-CD3ε antibody (5 μg/ml in PBS) (BioLegend, 100340) for 4 h at 37 °C prior to cell seeding. Cells were then cultured in RPMI 1640 medium with anti-CD28 antibody (2 μg/ml) (eBioscience, 16-0281-85). After 48 h of incubation, T cells were activated.

2.5. T cell migration assay

T cells were stimulated with anti-CD3ε and anti-CD28 antibodies (48 h) for activation, labeled with PKH26 (Sigma-Aldrich, USA) and seeded into the upper chamber of a Transwell plate (2×10^5/well). TDN$_{FasL}$ and TDNs were labeled with FITC and added to the lower chamber of the plate. Pure MCP-1 was used as positive control. After 12 h, the plate was observed under a fluorescence microscope and the number of PKH26-labeled T cells in the lower chamber was quantified.

2.6. Apoptosis assay by flow cytometry

Apoptotic T cells were detected by staining with an anti-CD3-APC antibody (BioLegend, 100312), followed by a PE Annexin V Apoptosis Detection Kit (BD Biosciences, 559763). Briefly, cells were washed with cold PBS after CD3 staining for 30 min on ice and resuspended in binding buffer with 5 μl of PE Annexin V and 5 μl of 7-AAD solution. After incubation for 15 min, 400 μl of binding buffer was added to each tube. Samples were analyzed with a flow cytometer within 1 h. The apoptotic rate is the sum of AnnexinV$^+$/7-AAD$^+$ double-positive cells and AnnexinV$^+$/7-AAD$^-$ cells.

Table 1
Composition of nanoparticles used in this manuscript.

Abbreviation	Construction	Conjugated biomolecules
MSNs	Mesoporous silica nanoparticle	None
TDN$_{MCP-1}$		MCP-1
TDN$_{FasL}$		FasL
TDN$_S$		FasL and MCP-1

2.7. Flow cytometry analysis

For analysis of surface markers, a single-cell suspension from mouse spleens was stained with anti-CD4-PE/Cy7 antibody (BioLegend, 100528) or anti-CD25-APC antibody (BioLegend, 102012) for 30 min on ice in the dark. After fixation and permeabilization with a True-Nuclear Transcription Factor Buffer Set (BioLegend, 424401), cells were stained with *anti*-Foxp3-PE antibody (eBioscience, 126404) for detection of Tregs. For intracellular cytokine measurement, cells were incubated with Cell Activation Cocktail (BioLegend, 423303) at 37 °C in the dark for 6 h. *Anti*-IL-17-PE antibody (eBioscience, 12-7177-81) was used to determine intracellular expression of IL-17. The percentages of positive cells were determined with a flow cytometer (Cytomics FC 500; Beckman-Coulter) and analyzed using FlowJo_V10 software.

2.8. Protein isolation and Western blot analysis

Protein samples were extracted using RIPA buffer supplemented with protease inhibitor. Total protein concentration was assessed with BCA protein assay reagent (Beyotime, China). Thirty micrograms of each sample were loaded and separated by 8–12% SDS-PAGE, and transferred onto PVDF membranes (Millipore, Germany). The membranes were blocked in 5% BSA for 2 h at room temperature, followed by incubation overnight at 4 °C with primary antibodies against Fas (Santa Cruz Biotechnology, sc-1023), Caspase-3 (Cell Signaling Technology, 9662S), Bax (Cell Signaling Technology, 2772), Bcl-2 (Cell Signaling Technology, 2870), ALP (R&D Systems, AF2910), Runx2 (Cell Signaling Technology, 12556), CD11b (Abcam, ab133357), CD44 (Abcam, ab189524), CD3 (Santa Cruz Biotechnology, sc-20047), iNOS (Cell Signaling Technology,13120S), CD206 (Abcam, ab125028), GAPDH (CWBIO, CW0100), β-actin (CWBIO, CW0096), and β-tubulin (CWBIO, CW0098). After washing in PBST (PBS containing 0.1% Tween 20) three times, membranes were incubated with secondary antibodies for 2 h at room temperature. After incubation, membranes were washed in PBST. Blots were imaged with a Western-Light Chemiluminescent Detection System (Tanon, China). Quantification of digital images was performed using ImageJ software.

2.9. Enzyme-linked immunosorbent assay (ELISA)

For serum samples, peripheral blood samples were collected from mice and left for 2 h at room temperature before centrifuging for 20 min at 2000 g. Serum was removed, and samples were stored at −80 °C. For the cell culture supernatant, precipitates were removed by centrifugation. Mouse TGF-β, IL-17, IL-6, IL-10, TNF-α and IFN-γ (Neobioscience, China) were detected using ELISA kits according to the manufacturer's instructions.

2.10. OVX-induced osteoporosis and treatment

Female C57BL/6 mice were ovariectomized or sham-operated at ten weeks of age as previously described [19]. Briefly, after mice were weighed and anaesthetized, the external oblique muscle was dissected and a bilateral ovariectomy was performed to induce osteoporosis. Sham-operated mice, which underwent laparotomy, but in which the ovaries were left intact, served as controls. One month later, femurs of mice were isolated after euthanasia for micro-CT scanning to confirm estrogen deficiency-induced osteoporosis. PBS (200 μl), TDN$_{MCP-1}$ (20 mg/kg in 200 μl PBS), TDN$_{FasL}$ (20 mg/kg in 200 μl PBS), TDNs (20 mg/kg in 200 μl PBS) or ApoEVs (10 mg/kg in 200 μl PBS) was injected into OVX mice via the tail vein at 4 weeks post OVX (mice were treated only once during the experiment). Mice were sacrificed 8 weeks-post OVX for further examination.

2.11. Micro-CT analysis of the distal femur

High-resolution micro-CT analyses were performed on distal femurs from each mouse using explore Locus SP Pre-Clinical Specimen micro-computed tomography (GE Healthcare, USA). The scanner was set at a tube voltage of 80 kVp, a tube current of 80 μA and a voxel size of 16 μm^3. The exposure time was 3000 ms. The reconstruction and 3D quantitative analysis were performed using software provided by a desktop micro-CT system (GE Healthcare, USA). The same conditions were used for all samples. The region of interest (ROI) was 0.5 mm away from the growth plate, the height was 1.2 mm, and the cortical region was excluded. Bone mineral density (BMD, mg/cm^3), trabecular number (Tb. N, 1/mm), bone volume to tissue volume (BV/TV), and trabecular separation (Tb. Sp, mm) were quantitatively analyzed from the reconstruction data in the defined ROIs.

2.12. Isolation and characterization of mouse BMMSCs

BMMSCs were isolated from the femurs and tibias of sham-operated mice or OVX mice treated with PBS, TDN$_{MCP-1}$, TDN$_{FasL}$, or TDNs. Femurs and tibias were dissected out and cleaned of connective tissue. Cells were flushed out from long bones by a syringe with α-MEM supplemented with 20% FBS, 2 mM L-glutamine (Sigma-Aldrich, USA), and 1% penicillin/streptomycin (Invitrogen, USA). Single-cell suspensions were seeded in dishes and initially maintained in an atmosphere of 5% CO_2 at 37 °C. The medium was changed every 3 days. After reaching 80% confluence, cells were passaged using 0.25% trypsin.

Cell surface markers of BMMSCs were detected by flow cytometry analysis. Cells were harvested and washed in PBS. Then, the single-cell suspension was incubated with mouse anti-CD105-APC (BioLegend, 120413), anti-CD11b-FITC (BioLegend, 101206), anti-CD45-PE (eBioscience, 12-0451), anti-CD29-APC (eBioscience, 17-0291-82) and anti-CD34-PE (BioLegend, 119307) antibodies. Finally, cells were washed twice in PBS, subjected to flow cytometry analysis with a flow cytometer (Cytomics FC 500; Beckman-Coulter) and analyzed with FlowJo_V10 software.

2.13. In vitro osteogenic differentiation

BMMSCs were cultured in 6-well or 12-well plates at a density of 1×10^5 cells/ml per well. When cells reached 80-90% confluence, the growth medium was changed to osteogenic differentiation medium: α-MEM with 20% FBS, 1% penicillin/streptomycin, 5 mM β-glycerophosphate, 50 μg/ml ascorbic acid and 10 nM dexamethasone (Sigma-Aldrich, USA). The medium was refreshed every other day. For RT-PCR or Western blot assays, cells were differentiated for 5 or 10 days with osteogenic differentiation medium. For alizarin red staining, cells were differentiated for 21 days.

2.14. RNA extraction and real-time PCR

Total RNA was extracted using TRIzol reagent (Invitrogen, USA) according to the manufacturer's instructions. One microgram of RNA was reverse-transcribed with a PrimeScript RT reagent kit (Takara, Japan). Real-time (RT)-PCR was performed using a Quantitative SYBR Green Kit (Takara, Japan) and detected by CFX 96Touch (Bio-Rad). GAPDH was used as a loading control for quantitation of mRNA. Relative gene expression was calculated by the $\Delta\Delta-CT$ method. Primers for mRNA are listed below: ALP (Forward: 5′-CCAACTCTTTTGTGCCA-GAGA-3′; Reverse: 5′-GGCTACATTGGTGTTGAGCTTTT-3′), Runx2 (Forward: 5′-GACTGTGGTTACCGTCATGGC-3′; Reverse: 5′-ACTTGGTTTTTCATAACAGCGGA-3′); and GAPDH (Forward: 5′-TGTGTCCGTCGTGGATCTGA-3′; Reverse: 5′-TTGCTGTTGAAGTCG-CAGGAG-3′).

2.15. Alizarin red staining

Alizarin red staining of BMMSCs was performed 21 days after osteogenic induction. Cells were washed with PBS twice and fixed in 60% isopropanol for 15 min. Cells were then stained with 1% Alizarin Red (Sigma-Aldrich, USA) for 3 min at room temperature. To quantify the stain, we used 2% cetylpyridinium chloride (Sigma-Aldrich, USA) to elute the stain for 10 min and measured the absorbance at 540 nm.

2.16. Isolation of apoptotic extracellular vesicles (ApoEVs)

Activated T cells were treated with TDNs for 12 h to induce apoptosis. The cell supernatant was collected and centrifuged at 800 g for 10 min. The supernatant was transferred to a new tube and centrifuged at 16000 g for 30 min to concentrate ApoEVs in the pellet. The supernatant was removed, and the pellet was resuspended in PBS for subsequent experiments. The concentration of ApoEVs was determined using a BCA protein assay kit (Beyotime, China).

2.17. Characterization of ApoEVs

The size distribution of ApoEVs was detected using a Zetasizer Nano ZSE (Malvern, UK). The morphology of ApoEVs was observed by scanning electron microscope (SEM) (Hitachi, Japan). Identification of Annexin V and C1q in ApoEVs was conducted using an Annexin V-FITC/PI apoptosis assay kit (7Sea Biotech, A005-2) or anti-mouse C1q antibody (CL7501F, CEDARLANE). Fluorescence images were captured with CLSM (Nikon, Japan). Western blotting was performed to characterize protein constitution of the ApoEVs. Protein samples were extracted from T cells, apoptotic T cells and ApoEVs.

2.18. Isolation and characterization of mouse bone marrow derived macrophages (BMDMs)

Primary macrophages were derived from bone marrow-derived monocytes of C57BL/6 mice. Femurs and tibias were dissected out and cleaned of connective tissue. Cells were flushed out from long bones by a syringe with PBS followed by erythrocyte lysis in ACK lysis buffer. Cells were maintained in DMEM (high glucose) supplemented with 10% FBS, 1% penicillin/streptomycin and M-CSF (20 ng/ml) to induce maturation of macrophages. After induction for 7 days, cells were used in subsequent experiments. Induction of mature macrophages was evaluated by fluorescence staining of F4/80 and CD11b.

2.19. Immunomodulatory effects of T cell-derived apoptotic extracellular vesicles in vitro

Macrophages were treated with TNF-α (500 ng/ml) to simulate an inflammatory environment *in vitro*. After 2 h, the medium was refreshed, and 25 μg/ml ApoEVs or an equal volume of PBS was added to the culture system (named the TNF-α+ApoEVs or TNF-α group). Macrophages without TNF-α stimulation were used as controls. Twenty-four hours later, the cell culture supernatant was collected to detect cytokines (TGF-β, IL-6, IL-10 and TNF-α) by ELISA. Expression levels of iNOS and CD206 were analyzed both by both Western blot and immunofluorescence staining.

2.20. Biosafety evaluation of TDNs

The biosafety evaluation of TDNs was conducted in C57BL/6 mice in response to PBS (200 μl), TDN$_{MCP-1}$, TDN$_{FasL}$, and TDNs (20 mg/kg in 200 μl PBS) administration. After 4 weeks, mouse serum samples were separated for biochemical index detection, and major organs were collected for hematoxylin-eosin (H&E) staining (Leica). Analysis of levels of serum ALT, AST, ALP, BUN, Crea and CK was performed by the clinical laboratory (Xijing Hospital, Fourth Military Medical University).

2.21. In vivo biodistribution and uptake of TDNs in liver

TDNs were labeled with 1,1′-Dioctadecyl-3,3,3′,3′-tetramethylindotricarbocyanine iodide (DiR). OVX mice were injected with PBS or DiR-labeled TDNs (20 mg/kg in 200 μl PBS) via tail vein. After 6, 24, 48 and

72 h, freshly dissected tissues (heart, liver, spleen, lung, kidney, and bone) were collected and analyzed for the fluorescence signal. The luminescence was acquired for a few seconds in an *ex vivo* IVIS imaging system (Xenogen).

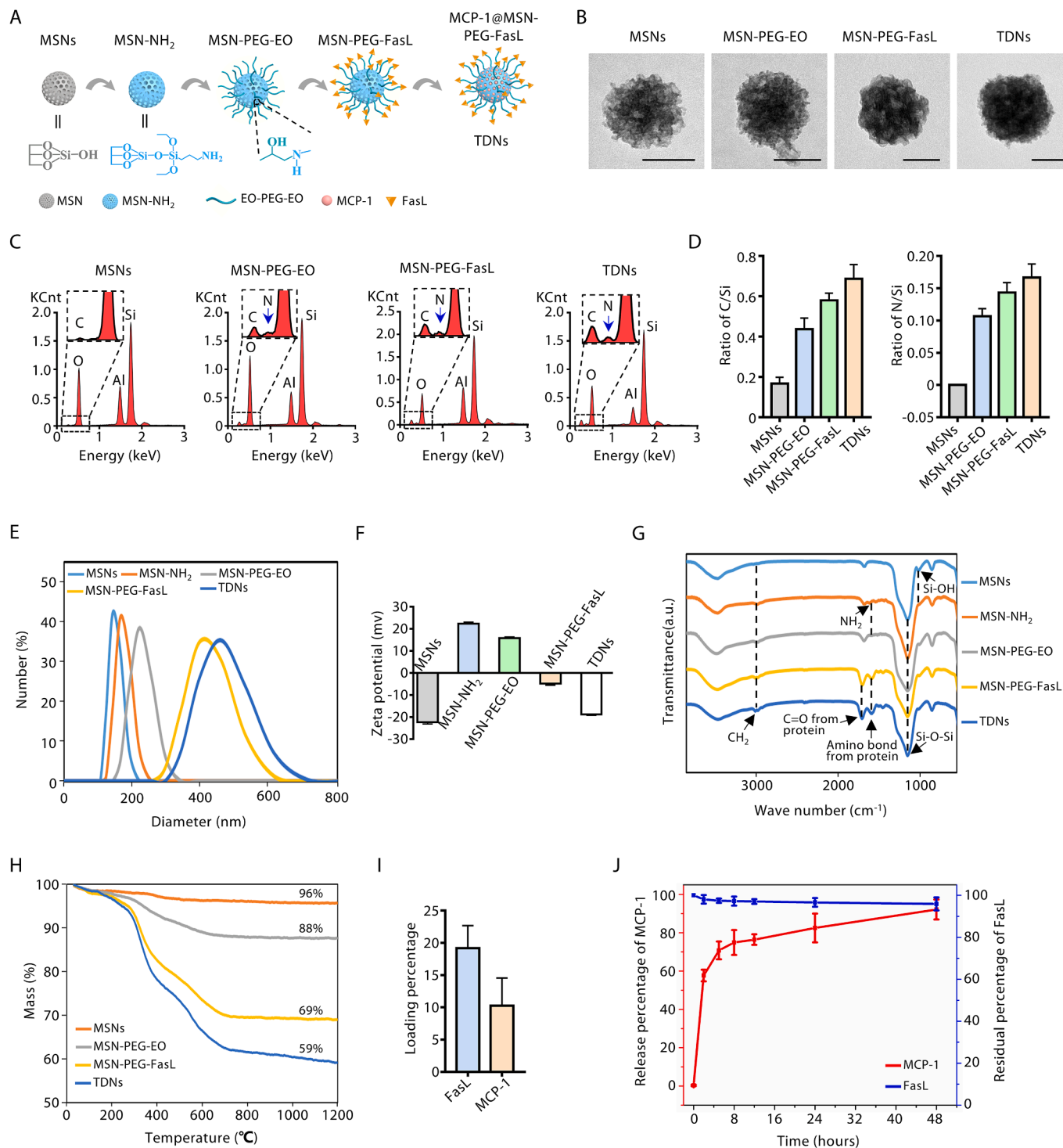For observation of the uptake of TDNs by macrophages *in vivo*, RhB-

Fig. 1. Synthesis and characterization of TDNs. (A) Schematic illustration of TDNs synthesis. TDNs: MCP-1@MSN-PEG-FasL (B) Transmission electron microscopy (TEM, scale bar = 100 nm) images and (C) energy-dispersive X-ray spectroscopy (EDX) of TDNs and the intermediate products (MSN, MSN-PEG-EO and MSN-PEG-FasL). (D) Element ratio of C/Si and N/Si in MSNs, MSN-PEG-EO, MSN-PEG-FasL and TDNs obtained from EDX results. (E) Size distribution, (F) surface charge analysis and (G) chemical composition analysis of TDNs and the intermediate products (MSN, MSN-NH₂, MSN-PEG-EO and MSN-PEG-FasL) investigated by dynamic light scattering (DLS) (E), zeta potential measurements (F) and Fourier-transform infrared spectroscopy (G). (H) Thermogravimetric analysis (TGA) of the MSNs, MSN-PEG-EO, MSN-PEG-FasL and TDNs. (I) Loading percentages of FasL and MCP-1 in TDNs calculated from the TGA results. (J) The release profiles of MCP-1 from TDNs in PBS buffer and the preservation rate of FasL on TDNs against incubation time in PBS buffer. n = 3 per group. Data are presented by mean ± SD.

labeled TDNs (20 mg/kg in 200 μl PBS) were injected into OVX mice via tail vein. After 6 h, mice were euthanized. The liver was obtained and fixed with 4% PFA overnight. Frozen sections were prepared, and slides were stained with *anti*-F4/80 (Abcam, ab6640) antibodies, followed by Hoechst staining. The fluorescence imaging was performed by CLSM.

2.22. Statistical analysis

Statistical analysis was performed using SPSS software. For all

graphs, data were represented as the mean ± SD. Statistical significance of differences between two data sets was calculated by the two-tailed unpaired Student's *t*-test; for comparison of multiple groups, the one-way ANOVA test was performed followed by Tukey's HSD test for multiple post hoc comparisons. The number of samples per group (n) was marked in the figure legends. P-values less than 0.05 were considered statistically significant.
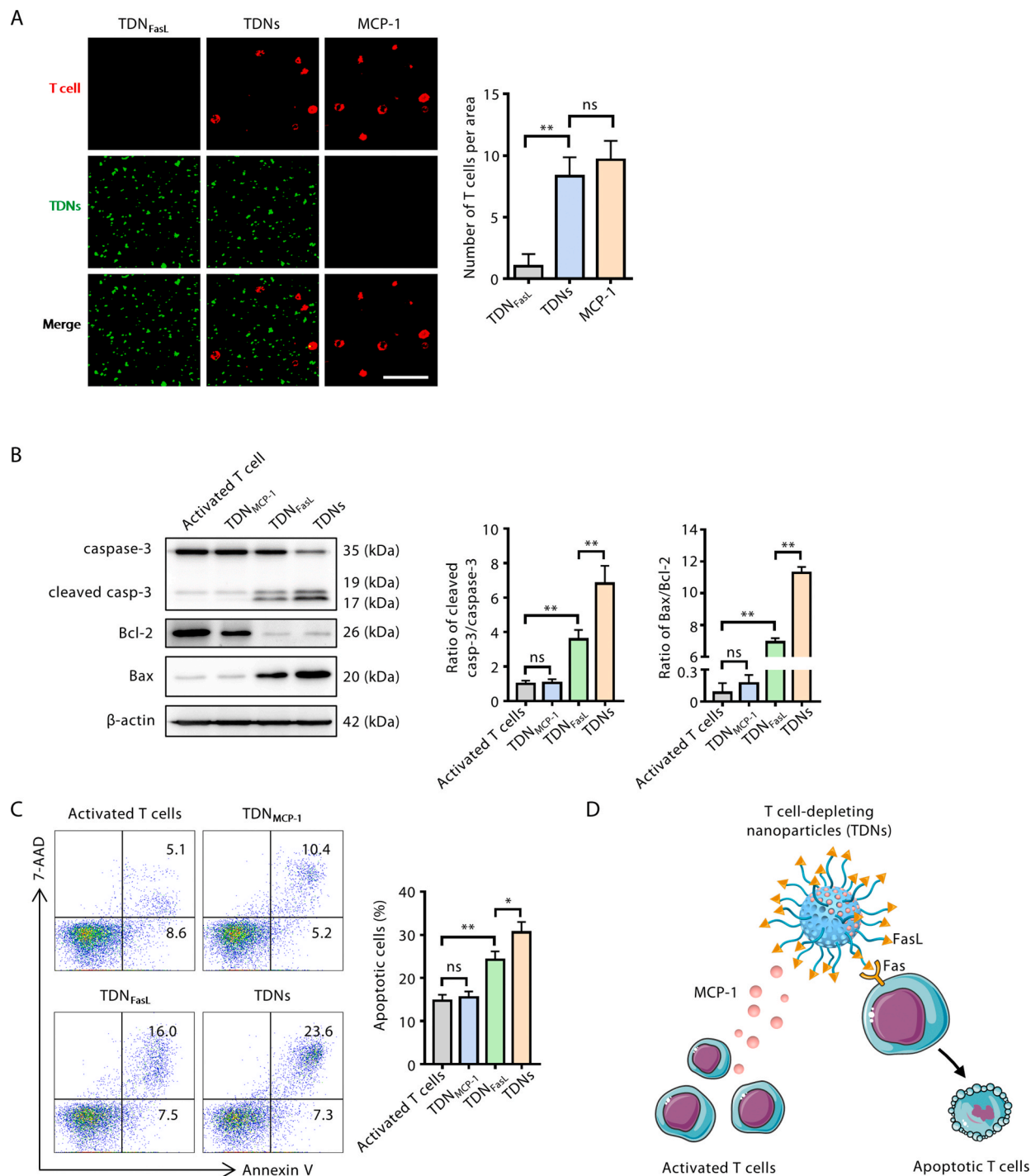

Fig. 2. *In vitro* recruitment and apoptosis of activated T cells by TDNs. (A) Recruitment of activated T cells (PKH26 labeled, red) by TDN_FasL or TDNs (FITC labeled, green) in a Transwell coculture system (scale bar = 50 μm). (B) Western blotting analysis of expression of apoptosis-related proteins. Grey values of cleaved caspase-3 to caspase-3 and Bax to Bcl-2 were calculated. (C) Flow cytometry analysis of apoptotic activated T cells. (D) Schematic diagram showing the mechanism of TDN-induced activated T cell apoptosis. n = 3 per group. Data are presented by mean ± SD; ns, not significant; *P < 0.05; **P < 0.01 by one-way ANOVA.

3. Results

3.1. Synthesis and characterization of T cell-depleting mesoporous silica nanoparticles (TDNs)

The synthesis of TDNs was diagramed in Fig. 1A. The stepwise formation of TDNs was directly determined by transmission electron microscope (TEM, Fig. 1B). As shown in Fig. 1B, the TDNs maintained a spherical structure during fabrication, and gradually exhibited generation of organic shells and indistinctness of porous structures (Fig. 1B). Compared to MSNs, a new characteristic peak of N appeared in MSNs-PEG-EO, MSN-PEG-FasL and TDNs (Fig. 1C) and the ratios of C/Si and N/Si increased gradually (Fig. 1D). These results indicated the successful conjugation of FasL onto the surface of TDNs and encapsulation of MCP-1 in their pores. The size and surface charge of the resulting TDNs and the intermediate products during fabrication were also investigated, which shows proper size increase (Fig. 1E) and charge changes (Fig. 1F) in good accordance with the hydrodynamic radius and electronic properties of certain components (Fig. 1E–F). Further evidence about the chemical structure of TDNs was provided by Fourier transform infrared (FTIR) spectrometry, which showed the characteristic signal of Si-O-Si from MSNs, the N-H signal from amino acids, and C=O from FasL and MCP-1 as the design (Fig. 1G).

To evaluate the therapeutic efficiency of TDNs, the maximum loading percentages of FasL and MCP-1 were investigated (Fig. 1H–I). The results showed that up to approximately 20 wt% FasL and 10 wt% MCP-1 could be conjugated/encapsulated in TDNs for further therapy. As expected, the encapsulated MCP-1 rapidly escaped from TDNs in 48 h, ending with a cumulative release of over 90% (Fig. 1J). The conjugated FasL was well maintained on the surface of TDNs, which only lost less than 5% even after 48 h of incubation under simulated physiological conditions (PBS with pH 7.4).

3.2. The effect of TDNs on recruitment and apoptosis of activated T cells in vitro

We first investigated the biological function of TDNs *in vitro*. Activated T cells were much larger than unactivated T cells (Fig. S1A). In addition, expression of CD25 and Fas was elevated in activated T cells compared to unactivated T cells (Figs. S1B–C). A Transwell coculture system was used to verify the chemotactic response of activated T cells to the TDNs (Fig. 2A). The results revealed that some of the activated T cells migrated into the lower chamber of the plate in the TDNs and MCP-1 groups, suggesting that TDNs recruit activated T cells. However, in the TDN$_{FasL}$ (TDNs without loading of MCP-1, referring to MSN-PEG-FasL in Fig. 1) group, almost no T cells were found in the lower chamber, indicating that MCP-1 is an essential component for TDNs to recruit T cells.

Subsequently, the ability of TDNs to induce apoptosis of activated T cells was examined. Expression of apoptosis-related proteins, including caspase-3, Bcl-2 and Bax was detected (Fig. 2B). Compared to the non-treated activated T cells, the ratios of cleaved-caspase-3 to caspase-3 and Bax to Bcl-2 were elevated in the TDN$_{FasL}$ (TDNs without loading of MCP-1) and TDNs groups, indicating the apoptosis of activated T cells in these two groups. However, importantly, the TDNs exerted a greater effect than the TDN$_{FasL}$. In addition, TDN$_{MCP-1}$ (TDNs without loading of FasL) showed no changes in expression of these proteins, as expected.

The apoptotic rates of activated T cells were also determined by flow cytometry (Fig. 2C). Similar to the results of apoptosis-related protein expression showed by western blotting, the apoptotic rates of activated T cells were dramatically increased in the TDN$_{FasL}$ and TDNs groups compared to the nontreated activated T cell group. In addition, the apoptotic rate of T cells in the TDNs group was significantly higher than in the TDN$_{FasL}$ group. These data suggest that MCP-1 mediates the recruitment of activated T cells, which significantly enhances the ability of the TDNs to induce T cell apoptosis. Similarly, the TDN$_{MCP-1}$ group

showed no changes in the apoptotic rate (Fig. 2C). Taken together, these results reveal that the TDNs effectively recruited activated T cells by MCP-1 and induce their apoptosis through the Fas/FasL interaction *in vitro* (Fig. 2D).

3.3. TDNs induced immune tolerance in OVX mice

Activated T cells play a key role in the interplay between bone and the immune system. Under estrogen deficiency conditions, T cells are overactivated, and they secrete pro-osteoclastogenic factors, which exacerbate bone loss. As we verified that TDNs recruit activated T cells and induce their apoptosis *in vitro*, we hypothesized that TDNs would induce apoptosis of activated T cells and achieve therapeutic effects on OVX mice, representing a reliable estrogen-deficient osteoporosis animal model.

Female C57BL/6 mice received bilateral ovariectomy surgery to establish an estrogen deficiency-induced osteoporosis model. Four weeks after the OVX surgery, femur bone mass was markedly decreased in OVX mice compared to sham mice (Fig. S2A). OVX mice exhibited significantly decreased bone mineral density (BMD), bone volume to tissue volume (BV/TV) and trabecular number (Tb. N), along with an increase in trabecular separation (Tb. Sp) (Fig. S2B). These results all confirmed the successful establishment of the estrogen deficiency-induced osteoporosis model. Four weeks after OVX surgery, mice were intravenously injected with PBS, TDN$_{MCP-1}$, TDN$_{FasL}$, or TDNs (Fig. 3A). The percentage of CD3$^+$ T cells in peripheral blood mononuclear cells (PBMCs) and their apoptotic rate were tested 6 h after injection. We observed that only TDNs-treated mice exhibited significantly lower proportions of CD3$^+$ T cells (Fig. 3B) with obvious elevation of apoptotic CD3$^+$ T cells among all other groups (Fig. 3C). However, TDN$_{MCP-1}$ or TDN$_{FasL}$ was unable to decrease CD3$^+$ T cells or induce T cell apoptosis (Fig. 3B–C).

It has been reported that in the cases of estrogen deficiency, T cell subset distribution, especially the Treg/Th17 balance, is disturbed [6,7]. Moreover, the engulfment of apoptotic T cells by phagocytes, such as macrophages, trigger the production of TGF-β to induce Tregs which result in immune tolerance. Therefore, we assessed the populations of splenic Th17 cells (Fig. 3D) and Tregs (Fig. 3E) eight weeks post-ovariectomy. As shown in Fig. 3, the percentage of Th17 cells was decreased while Tregs were increased in the TDNs-treated group. In contrast, no obvious changes were observed in either the TDN$_{MCP-1}$ or TDN$_{FasL}$ group (Fig. 3D–E). The level of the proinflammatory cytokines in the serum was also tested. Results showed that concentrations of IFN-γ, IL-17 and TNF-α were all decreased in the TDNs group compared with that in the PBS group. These data collectively indicate that the TDNs treatment provides an immune tolerant environment for OVX mice as shown by elevated Tregs and decreased proinflammatory cytokines.

3.4. TDNs administration ameliorates the osteopenia phenotype and rescues the osteogenic deficiency of bone marrow mesenchymal stem cells (BMMSCs) in OVX mice

To determine whether treatment with TDNs ameliorates the osteopenia phenotype, we analyzed the bone mass of femurs using micro-CT four weeks after treatment (Fig. 4A). Micro-CT scanning revealed that TDNs administration resulted in a marked elevation of BMD, BV/TV, and Tb. N with a decrease in Tb. Sp compared to the PBS group. However, the TDN$_{MCP-1}$ and TDN$_{FasL}$ groups exhibited no significant change in bone mass compared to the PBS group (Fig. 4B). To further investigate the osteogenic ability of BMMSCs, we isolated sham and OVX BMMSCs from bone marrow. The cells exhibited characteristic patterns of mesenchymal stem cell surface markers, including CD105 and CD29 whereas the hematopoietic markers CD11b, CD45 and CD34 were negative (Fig. S2C). We next compared the osteogenic differentiation abilities of BMMSCs from sham and OVX mice. Alizarin red staining
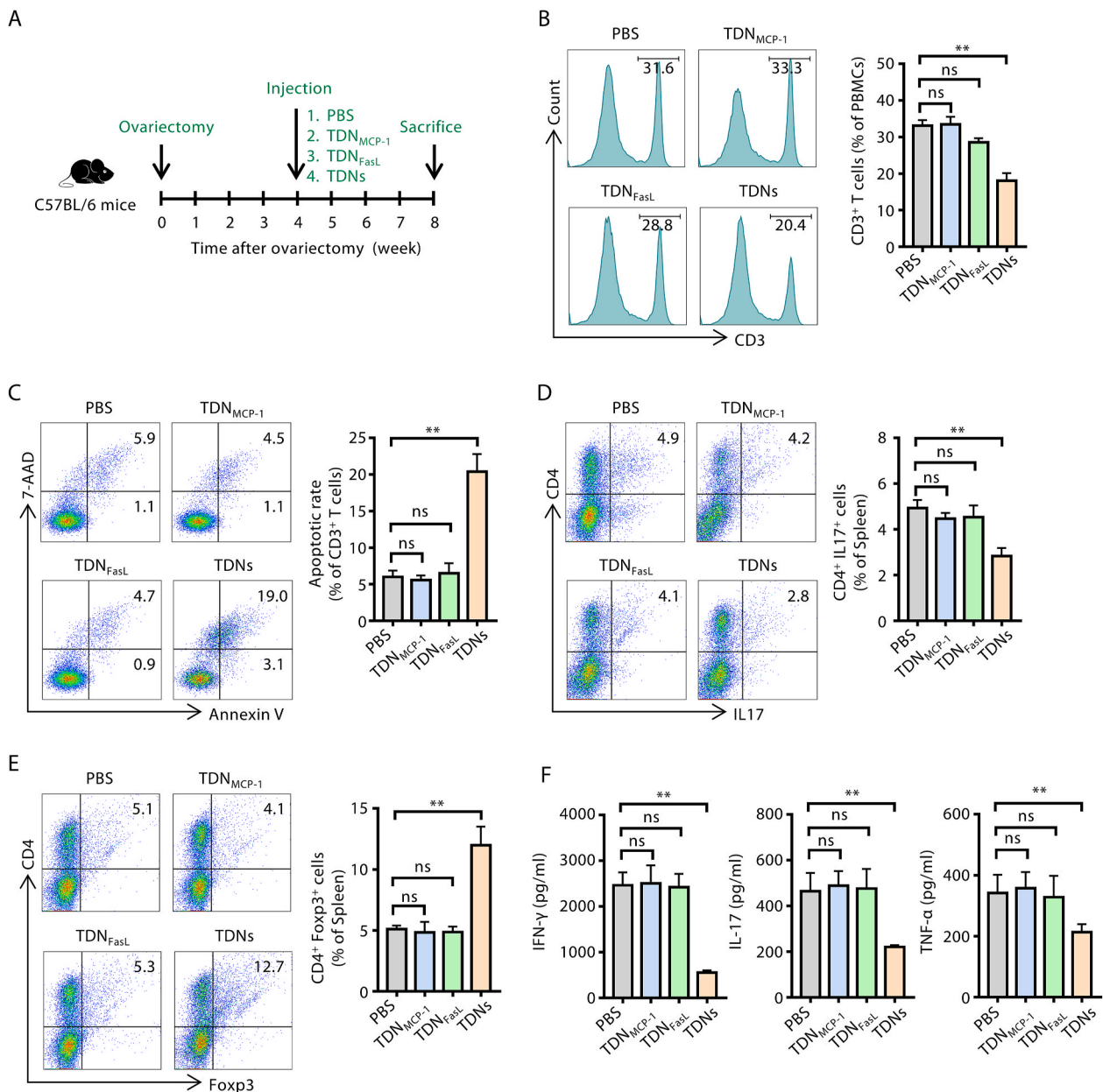
Fig. 3. TDNs induce immune tolerance in OVX mice. (A) Schematic showing multiple treatments in OVX mice. Ten-week-old female C57BL/6 mice received ovariectomy surgery and were injected with PBS (200 µl), TDN_MCP-1, TDN_FasL, or TDNs (20 mg/kg in 200 µl PBS) 4 weeks after ovariectomy. Mice were sacrificed 8 weeks post-ovariectomy for further examination. (B) Frequencies of CD3$^+$ T cells in OVX mice 6 h after injection. (C) Frequencies of apoptotic CD3$^+$ T cells 6 h after injection. (D) Frequencies of CD4$^+$/IL17$^+$ Th17 cells 8 weeks post-ovariectomy. (E) Frequencies of CD4$^+$/Foxp3$^+$ Tregs 8 weeks post-ovariectomy. (F) Serum concentrations of IFN-γ, IL-17 and TNF-α detected by ELISA. n = 6 per group. Data are presented as mean ± SD; ns, not significant; **P < 0.01 by one-way ANOVA.

showed that BMMSCs derived from OVX mice formed fewer mineralization nodules (Fig. S2E), exhibited reduced expression of ALP and Runx2, two markers of osteogenesis, at both the mRNA and protein levels (Figs. S2D and S2F). Next, we investigated whether TDNs could rescue the osteogenic deficiency of BMMSCs from OVX mice. The results showed that the gene expression levels of ALP and Runx2 were significantly higher in the TDN-treated group (Fig. 4C). Moreover, alizarin red staining revealed stronger osteoblast activity in the TDNs group than in the PBS group (Fig. 4D). Protein expression of ALP and Runx2 detected by western blotting also showed similar results (Fig. 4E). In contrast, no significant improvement in osteogenic differentiation was observed in BMMSCs from OVX mice that received TDN_MCP-1 or TDN_FasL therapy (Fig. 4C–E). This experimental evidence suggests that TDNs treatment inhibits bone loss and rescues the osteogenic deficiency of BMMSCs in

OVX mice.

3.5. Immunomodulatory effect of T cell-derived apoptotic extracellular vesicles (ApoEVs)

It has been established that during the apoptotic process, cells release large numbers of extracellular vesicles, called apoptotic extracellular vesicles (ApoEVs) [20–22]. Given that apoptotic cells release ApoEVs and that TDNs induce apoptosis of activated T cells *in vitro*, we hypothesized that the amount of ApoEVs released by apoptotic T cells would increase after TDNs treatment. We then isolated ApoEVs derived from activated T cells after treatment with TDN_MCP-1, TDN_FasL or TDNs. The concentration of ApoEVs in the TDN_FasL and TDNs groups increased significantly compared to activated T cells, while the TDNs group
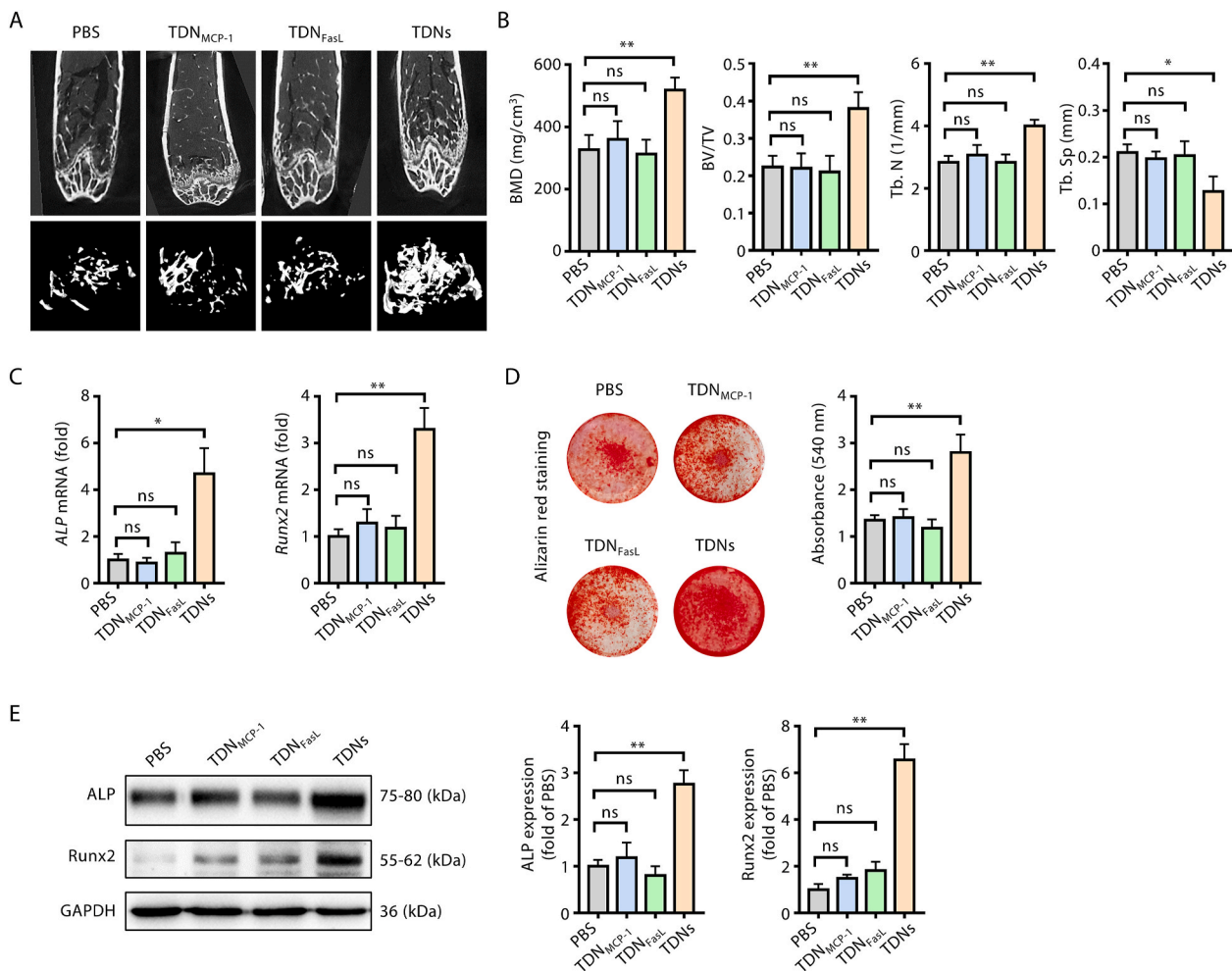
Fig. 4. TDNs administration inhibits bone loss and rescues the osteogenic deficiency of BMMSCs in OVX mice. (A) Micro-CT analysis of trabecular bone mass in the femurs. (B) Quantitative analysis of bone mineral density (BMD), bone volume to tissue volume (BV/TV), trabecular number (Tb. N) and trabecular separation (Tb. Sp). (C) BMMSCs from each group were isolated and cultured in osteogenic medium. Real-time PCR was performed to detect mRNA expression of *ALP* and *Runx2* on day 5 after osteogenic induction. (D) Alizarin red staining and quantification of mineralized nodules were performed on day 21 after induction. (E) Western blotting analysis and quantification of osteogenic related proteins ALP and Runx2 on day 10 after induction. n = 6 per group. Data are presented as mean ± SD; ns, not significant; *P < 0.05; **P < 0.01 by one-way ANOVA.

induced the highest production of ApoEVs (Fig. 5A). Expectedly, the amount of ApoEVs derived from TDN$_{MCP-1}$ treated T cells were no different from activated T cells (Fig. 5A), as we have shown above that TDN$_{MCP-1}$ does not induce the apoptosis of activated T cells (Fig. 2C). Scanning electron microscopy (SEM) revealed that ApoEVs were approximately 500 nm in diameter (Fig. 5B), consistent with the dynamic light scattering (DLS) results (Fig. 5C). We confirmed that these ApoEVs expressed the ApoEVs-specific surface markers Annexin V and C1q, as assayed by immunofluorescence staining (Fig. 5D). Western blotting confirmed that activated T cells, apoptotic T cells and apoptotic T cell-derived ApoEVs (T-ApoEVs) expressed major membrane proteins, including CD3, CD44 and CD11b (Fig. 5E). In addition, cleaved caspase-3, a specific marker of apoptotic cells, was also detectable in ApoEVs, indicating the retention of apoptotic components in ApoEVs (Fig. 5E).

Previous studies have revealed that engulfment of apoptotic cells by macrophages promotes their transformation towards the M2 phenotype [23]. Herein, to investigate the potential influence of ApoEVs on macrophage polarization, we isolated mouse bone marrow derived macrophages (BMDMs) and confirmed that almost all cells expressed macrophage-specific surface markers CD11b (Fig. S3A) and F4/80 (Fig. S3B). Then, BMDMs were treated with TNF-α *in vitro* to simulate the microenvironment of elevated TNF-α *in vivo* under OVX conditions [24].

CD206 was selected as a marker of M2-type macrophages and iNOS was selected as the M1-type macrophage marker. As seen from the confocal microscopy images, TNF-α increased the number of iNOS⁺ (M1) macrophages. However, after treatment with ApoEVs, the proportion of iNOS⁺ cells decreased while the proportion of CD206⁺ cells increased, indicating that more M2-type and fewer M1-type macrophages were generated (Fig. 5F). Consistent with the results of immunofluorescence staining in Fig. 5F, ApoEVs downregulated expression of iNOS and significantly increased levels of CD206 (Fig. 5G). Meanwhile, addition of TNF-α remarkably enhanced secretion of IL-6 and TNF-α compared to the control group. While ApoEVs inhibited the secretion of IL-6 and TNF-α, and promoted secretion of the anti-inflammatory factors, TGF-β and IL-10 (Fig. 5H). Taken together, this evidence demonstrates that T cell-derived ApoEVs have important immunoregulatory effects, which contribute to establishing an immune tolerant environment.

3.6. T cell-derived apoptotic extracellular vesicles participated in the amelioration of osteopenia by TDNs in OVX mice

Increasing evidence suggests that ApoEVs produced during apoptosis have important immunoregulatory roles. ApoEVs have been shown to promote tissue development and regeneration in multiple systems [22, 25–27]. Recently, a study reported a role of exogenous BMMSC-derived
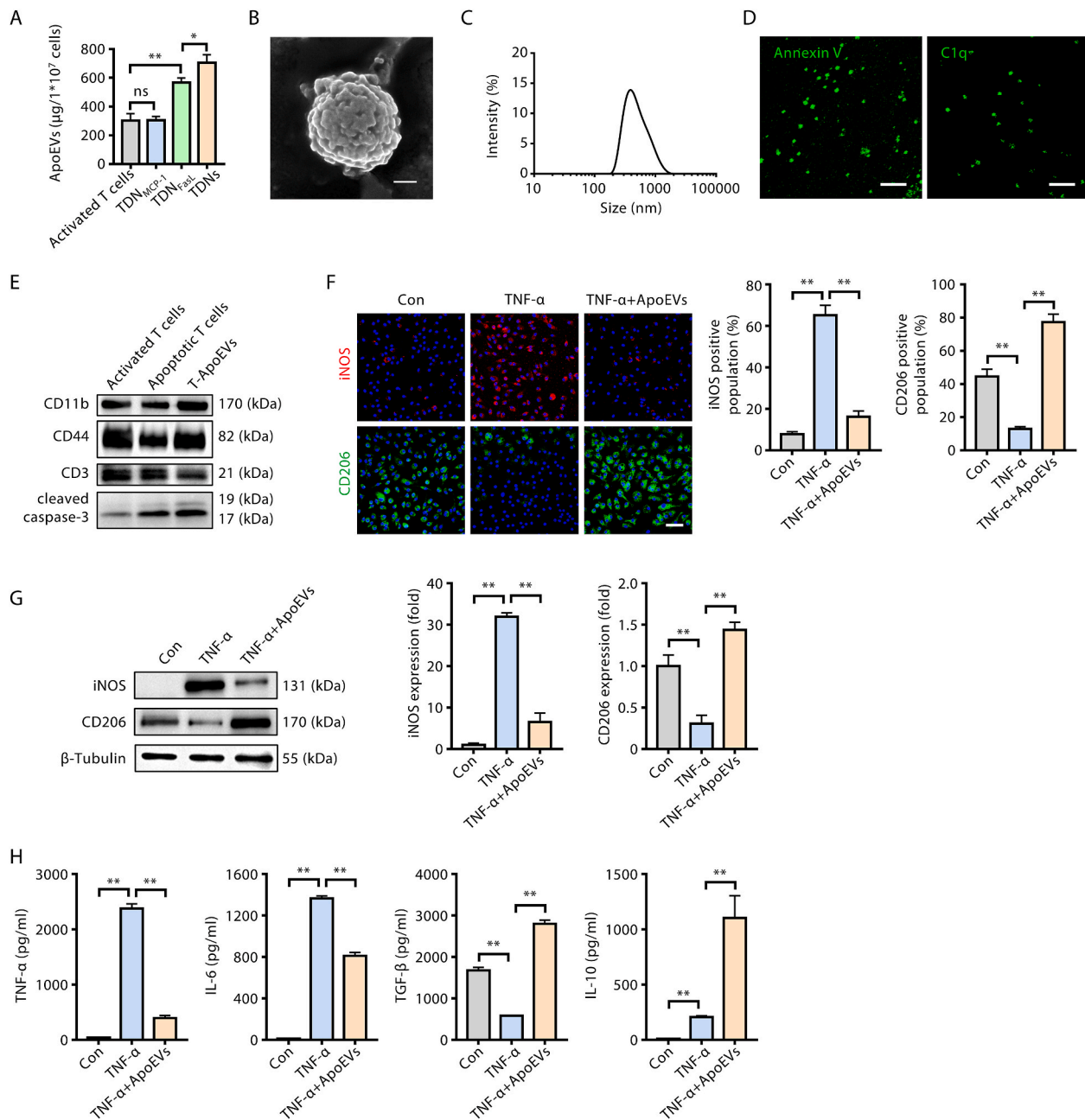
Fig. 5. Immunomodulatory effects of T cell-derived apoptotic extracellular vesicles (ApoEVs). (A) Quantification of T cell-derived ApoEVs after activated T cells were treated with TDNs for 12 h. (B) Representative scanning electron microscopy (SEM) image of T cell-derived ApoEVs (scale bar = 200 nm). (C) Size distribution of T cell-derived ApoEVs detected by dynamic light scattering (DLS). (D) Immunofluorescence staining of Annexin V and C1q in ApoEVs (scale bar = 5 μm). (E) Protein characterization of ApoEVs by western blotting. T-ApoEVs: T cells-derived ApoEVs. (F) Representative fluorescence images of the phenotypes of macrophages and the percentage of iNOS or CD206-positive populations; iNOS$^+$ (red) cells indicate the M1 phenotype, CD206$^+$ (green) cells indicate the M2 phenotype (scale bar = 50 μm). (G) Western blotting analysis of the phenotypic markers of macrophages. M1 marker: iNOS; M2 marker: CD206. (H) Concentrations of cytokines (TNF-α, IL-6, TGF-β and IL-10) in cell supernatants detected by ELISA. n = 3 per group. Data are presented as mean ± SD; ns, not significant; *P < 0.05; **P < 0.01 by one-way ANOVA.

ApoEVs in maintaining bone homeostasis and suggested the potential of ApoEVs to treat osteoporosis [22]. Because we demonstrated that T cell-derived ApoEVs participate in immune regulation *in vitro*, we wondered whether ApoEVs-induced immune tolerance could help restore the osteogenic ability of BMMSCs and improve osteopenia in OVX mice. OVX mice were administered PBS, TDNs or ApoEVs via tail vein injection four weeks after OVX surgery. Another four weeks later, the bone mass of femur was analyzed. Micro-CT scanning revealed that ApoEVs partially alleviated bone loss in OVX mice compared to the PBS group (Fig. 6A), which was also emphasized by the quantities of BMD,

BV/TV, Tb. N, and Tb. Sp (Fig. 6B). To investigate the differentiation potential of BMMSCs, we next cultured BMMSCs (derived from PBS, TDNs-or ApoEVs-treated OVX mice) in osteogenic differentiation medium. ApoEVs significantly enhanced expression of ALP and Runx2 at the mRNA and protein levels, although the effect of ApoEVs was not as strong as that of TDNs (Fig. 6C and E). A similar conclusion was drawn from the mineralized nodules reflected by alizarin red staining (Fig. 6D). The proportions of Th17 cells and Tregs in the spleen were also analyzed. After treatment with ApoEVs, the percentage of Th17 cells decreased while Tregs increased compared to the PBS group (Fig. 6F and
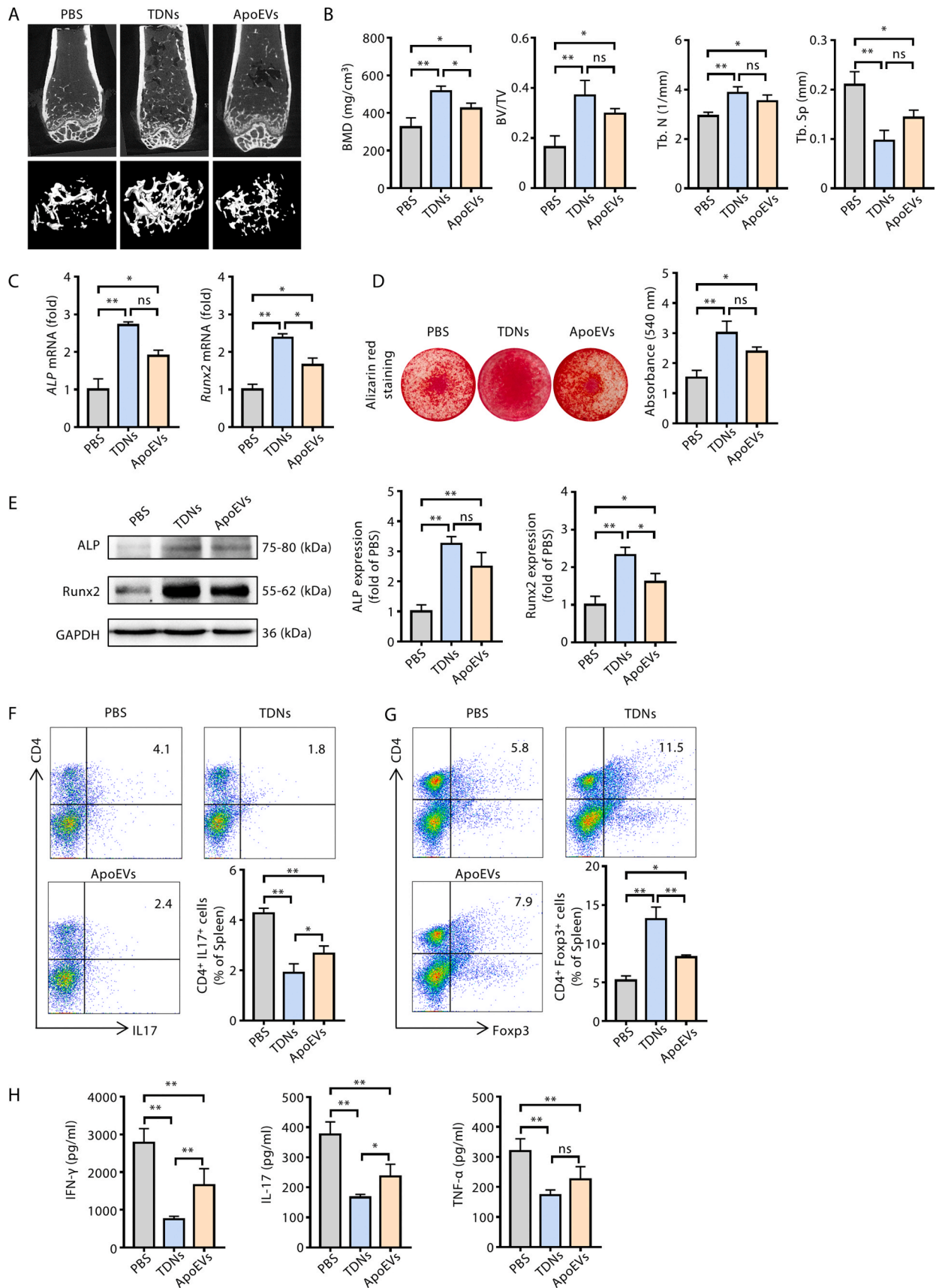
(caption on next page)

Fig. 6. T cell-derived apoptotic extracellular vesicles participate in the amelioration of osteopenia by TDNs in OVX mice. Ten-week-old female C57BL/6 mice received ovariectomy surgery and were injected with PBS (200 μl) or ApoEVs (10 mg/kg in 200 μl PBS) 4 weeks after ovariectomy. Mice were sacrificed 8 weeks post-ovariectomy for further examination. (A) Micro-CT analysis of trabecular bone mass in the femurs. (B) Quantitative analysis of BMD, BV/TV, Tb. N and Tb. Sp. (C) BMMSCs from each group were isolated and cultured in osteogenic medium. Real-time PCR was performed to detect mRNA expression of *ALP* and *Runx2* on day 5 after osteogenic induction. (D) Alizarin red staining and quantification of mineralized nodules were performed on day 21 after induction. (E) Western blotting analysis and quantification of the osteogenic-related proteins ALP and Runx2 on day 10 after induction. (F) Frequencies of CD4$^+$/IL17$^+$ Th17 cells 8 weeks post-ovariectomy. (G) Frequencies of CD4$^+$/Foxp3$^+$ Tregs 8 weeks post-ovariectomy. (H) Serum concentrations of IFN-γ, IL-17 and TNF-α detected by ELISA. n = 6 per group. Data are presented as mean ± SD; ns, not significant; *P < 0.05; **P < 0.01 by one-way ANOVA.

G). Moreover, ApoEVs blunted production of proinflammatory cytokines, IFN-γ, IL-17 and TNF-α (Fig. 6H), leading to a more suitable environment for improving osteopenia in OVX mice. In summary, these data suggest that ApoEVs play a role in the ameliorating osteoporosis and rescuing the osteogenic deficiency of BMMSCs in OVX mice in response to TDNs.

3.7. In vivo biodistribution and biosafety of TDNs

To determine the biodistribution of TDNs *in vivo*, DiR-labeled TDNs were injected in OVX mice via tail vein. As seen in Fig. S4A, the fluorescence intensity of TDNs in *ex vivo* tissue showed that TDNs were mainly distributed in the liver of OVX mice 6 h after injection (Fig. S4B), and they can quickly be up-taken by macrophages in the liver (Fig. S4B). The amount of TDNs in the liver gradually decreased and was almost invisible after 72 h, indicating that TDNs could be cleared after 72 h (Fig. S4A).

The biosafety of TDNs *in vivo* was also evaluated. The biochemical index showed no significant changes in alanine aminotransferase (ALT), aspartate aminotransferase (AST), alkaline phosphatase (ALP), blood urea nitrogen (BUN), creatinine (Crea), or creatine kinase (CK) between the PBS group and the other treated groups (Fig. S5A). Moreover, histological analysis revealed no apparent damage in the major organs (Fig. S5B). Taken together, these results provide compelling evidence that TDNs could be applied as a safe and effective formulation for immunoregulatory therapy.

4. Discussion

Osteoporosis is a common systemic skeletal disorder associated with ageing and the postmenopausal population, leading to bone fragility and increased risk of fracture [4,28]. Most current therapies for the prevention or treatment of osteoporosis focus on antiresorptive drugs. Despite the increasing kinds of effective drugs for osteoporosis, there remain several serious side effects, frustrating both doctors and patients, including the impairment of intrinsic repair mechanisms and the increased risk of atypical femur fractures [10]. Cross-talk has been shown to occur between the immune system and bone metabolism pathway, and T cells are actively involved in bone homeostasis [2].

It has been demonstrated that activated T cells contribute to elevated levels of proinflammatory cytokines under estrogen deficiency conditions. Since Fas is increasingly expressed in activated T cells than in naïve T cells and Fas-mediated apoptosis of T cells has long been known as a mechanism allowing the contraction of T-cell responses to prevent immunopathology [29], it is reasonable to hypothesize that the induction of activated T cell apoptosis represents a therapeutic modality. Fas expression has been detected in many types of cells, for example, thymus, liver, heart, lung, kidney and ovary [30]. Based on our results, TDNs were able to quickly release MCP-1 and induce the apoptosis of activated T cells in periphery. After that, TDNs were quickly be up-taken by macrophages in liver, and be cleared after 72 h, thus avoiding nonspecific apoptosis in other organs.

Our *in vitro* results revealed that TDNs could promote the migration of activated T cells and then effectively inducing their apoptosis. We extended this "recruitment and apoptosis" system to OVX mice, and found that TDNs also function to establish immune tolerance *in vivo*. Similar to some immunosuppressive regimens, we synthesized TNDs

aiming to inhibit the activation of the immune system and reduce chronic inflammation. However, excessive immunosuppressive are left susceptible to opportunistic infections and have increased risk of malignancies [31,32]. In the present study, we evaluated systemic toxicity/biosafety of TDNs in normal C57BL/6 mice for one month. Long-term test of chronic toxicity still needs to be accomplished. In addition, it is important to seek for new molecules that can selectively suppress or enhance immune responses by controlling the balance between Tregs and effector T cells.

The development of biomaterials with bioactivity offers new opportunities for manipulation of osteoporosis, and some studies have conducted preliminary exploration in OVX-induced osteoporosis [33, 34]. As one of the most frequently used nanocarriers, MSNs have been widely investigated for the delivery of various cargoes in nanomedicine [14,15,35]. Their high surface area, adjustable size and pore volume, good biocompatibility and biodegradability allow MSNs to be intensively applied as a reservoir for bioactive factors [36,37]. Nevertheless, nanoparticles often serve as delivery carriers of drugs to achieve targeted or long-term drug delivery [33,34]. In the present study, we designed another therapeutic mode that targeted the immune system to regulate abnormalities in bone metabolism. The TDNs described in this study function in the reconstruction of immune homeostasis by recruiting and killing activated T cells to induce immune tolerance, which has not previously been reported.

Apoptosis is an important biological process that is extensively involved in embryonic development, immune response, and tissue regeneration [38–41]. During apoptosis, cells secrete extracellular vesicles known as ApoEVs [42]. While it has been well established that extracellular vesicles released from healthy cells exhibit immunomodulatory effects, ApoEVs released from apoptotic cells remain understudied. A recent study identifies a previously unknown role of ApoEVs in maintaining MSC and bone homeostasis in both physiological and pathological contexts [22]. Besides, a biological effect of MSC-derived ApoEVs on tissue repair was reported in a myocardial infarction (MI) model [25]. They demonstrated MSC treatment for MI accompanied the production and release of ApoEVs derived from apoptotic MSCs, which enhanced angiogenesis and cardiac function recovery in MI rats. Consistent with these studies, apoptotic T cell-derived ApoEVs promoted tissue regeneration as well. Our data revealed that T cell-derived ApoEVs promoted polarization of macrophages towards the M2 phenotype. ApoEVs help restore the osteogenic ability of impaired BMMSCs and improve osteopenia in OVX mice. These evidences demonstrate that T cell-derived ApoEVs contribute to establishing an immune tolerant environment and imply the potential use of ApoEVs to treat osteoporosis and other inflammation-related diseases. However, the detailed mechanisms of ApoEVs-induced immune tolerance and its application still need to be further investigated.

5. Conclusions

In conclusion, this study describes a T cell-depleting mesoporous silica nanoparticle that ameliorates osteopenia the phenotype and rescues the osteogenic deficiency of BMMSCs in OVX mice. We demonstrated that the precise design of the TDNs enables rapid release of MCP-1 to recruit activated T cells and then induces their apoptosis through the conjugated FasL on the TDNs surface. Apoptotic signals recognized by macrophages help to skew the Treg/Th17 cell balance and create an

immune tolerant state. Thus, TDNs represent an efficient therapeutic method that eliminates activated T cells and establishes immune tolerance. This study lays the foundation for the treatment of osteoporosis and provides a promising therapeutic strategy for other immune disorders caused by excessive activated T cells.

Declaration of competing InterestCOI

The authors declare that they have no competing interests.

CRediT authorship contribution statement

Xiaoshan Yang: Investigation, Writing – original draft, Validation. **Fuxing Zhou:** Investigation, Formal analysis. **Pingyun Yuan:** Investigation, Writing – original draft, Data curation. **Geng Dou:** Investigation, Formal analysis. **Xuemei Liu:** Methodology. **Siying Liu:** Funding acquisition. **Xiangdong Wang:** Methodology. **Ronghua Jin:** Formal analysis. **Yan Dong:** Investigation, Funding acquisition. **Jun Zhou:** Funding acquisition. **Yajie Lv:** Resources. **Zhihong Deng:** Funding acquisition. **Shiyu Liu:** Writing – review & editing, Funding acquisition. **Xin Chen:** Writing – review & editing, Conceptualization. **Ying Han:** Supervision. **Yan Jin:** Supervision, Funding acquisition.

Acknowledgements

Appendix A. Supplementary data

Supplementary data to this article can be found online at https://doi.org/10.1016/j.bioactmat.2021.02.034.

References

[1] R. Eastell, T.W. O'Neill, L.C. Hofbauer, B. Langdahl, I.R. Reid, D.T. Gold, et al., Postmenopausal osteoporosis, Nat Rev Dis Primers 2 (2016) 16069, https://doi.org/10.1038/nrdp.2016.69.

[2] H.Y. Dar, Z. Azam, R. Anupam, R.K. Mondal, R.K. Srivastava, Osteoimmunology: the Nexus between bone and immune system, Front Biosci (Landmark Ed) 23 (2018) 464–492, https://doi.org/10.2741/4600.

[3] M. Tsukasaki, H. Takayanagi, Osteoimmunology: evolving concepts in bone-immune interactions in health and disease, Nat. Rev. Immunol. 19 (10) (2019) 626–642, https://doi.org/10.1038/s41577-019-0178-8.

[4] M.N. Weitzmann, R. Pacifici, Estrogen deficiency and bone loss: an inflammatory tale, J. Clin. Invest. 116 (5) (2006) 1186–1194, https://doi.org/10.1172/JCI28550.

[5] W. Zhang, K. Dang, Y. Huai, A. Qian, Osteoimmunology: the regulatory roles of T lymphocytes in osteoporosis, Front. Endocrinol. 11 (2020) 465, https://doi.org/10.3389/fendo.2020.00465.

[6] Y. Tanaka, Clinical immunity in bone and joints, J. Bone Miner. Metabol. 37 (1) (2019) 2–8, https://doi.org/10.1007/s00774-018-0965-5.

[7] H.Y. Dar, P. Shukla, P.K. Mishra, R. Anupam, R.K. Mondal, G.B. Tomar, et al., Lactobacillus acidophilus inhibits bone loss and increases bone heterogeneity in osteoporotic mice via modulating Treg-Th17 cell balance, BoneKEy Rep. 8 (2018) 46–56, https://doi.org/10.1016/j.bonr.2018.02.001.

[8] M.K. Park, J.S. Park, E.M. Park, M.A. Lim, S.M. Kim, D.G. Lee, et al., Halofuginone ameliorates autoimmune arthritis in mice by regulating the balance between Th17 and Treg cells and inhibiting osteoclastogenesis, Arthritis Rheum. 66 (5) (2014) 1195–1207, https://doi.org/10.1002/art.38313.

[9] J. Geng, S. Yu, H. Zhao, X. Sun, X. Li, P. Wang, et al., The transcriptional coactivator TAZ regulates reciprocal differentiation of TH17 cells and Treg cells, Nat. Immunol. 18 (7) (2017) 800–812, https://doi.org/10.1038/ni.3748.

[10] S. Khosla, L.C. Hofbauer, Osteoporosis treatment: recent developments and ongoing challenges, Lancet Diabet. Endocrinol 5 (11) (2017) 898–907, https://doi.org/10.1016/S2213-8587(17)30188-2.

[11] M. Khan, A.M. Cheung, A.A. Khan, Drug-related adverse events of osteoporosis therapy, Endocrinol Metab. Clin. N. Am. 46 (1) (2017) 181–192, https://doi.org/10.1016/j.ecl.2016.09.009.

[12] J.S. Suk, Q. Xu, N. Kim, J. Hanes, L.M. Ensign, PEGylation as a strategy for improving nanoparticle-based drug and gene delivery, Adv. Drug Deliv. Rev. 99 (Pt A) (2016) 28–51, https://doi.org/10.1016/j.addr.2015.09.012.

[13] S.M. Dadfar, K. Roemhild, N.I. Drude, S. von Stillfried, R. Knuchel, F. Kiessling, et al., Iron oxide nanoparticles: diagnostic, therapeutic and theranostic applications, Adv. Drug Deliv. Rev. 138 (2019) 302–325, https://doi.org/10.1016/j.addr.2019.01.005.

[14] S. Jafari, H. Derakhshankhah, L. Alaei, A. Fattahi, B.S. Varnamkhasti, A.A. Saboury, Mesoporous silica nanoparticles for therapeutic/diagnostic applications, Biomed. Pharmacother. 109 (2019) 1100–1111, https://doi.org/10.1016/j.biopha.2018.10.167.

[15] F. Tang, L. Li, D. Chen, Mesoporous silica nanoparticles: synthesis, biocompatibility and drug delivery, Adv. Mater. 24 (12) (2012) 1504–1534, https://doi.org/10.1002/adma.201104763.

[16] A. Yadav, V. Saini, S. Arora, MCP-1: chemoattractant with a role beyond immunity: a review, Clin. Chim. Acta 411 (21–22) (2010) 1570–1579, https://doi.org/10.1016/j.cca.2010.07.006.

[17] A. Strasser, P.J. Jost, S. Nagata, The many roles of FAS receptor signaling in the immune system, Immunity 30 (2) (2009) 180–192, https://doi.org/10.1016/j.immuni.2009.01.001.

[18] X. Chen, A.H. Soeriyadi, X. Lu, S.M. Sagnella, M. Kavallaris, J.J. Gooding, Dual bioresponsive mesoporous silica nanocarrier as an "AND" logic gate for targeted drug delivery cancer cells, Adv. Funct. Mater. 24 (44) (2014) 6999–7006, https://doi.org/10.1002/adfm.201402339.

[19] J. Huang, H. Yin, S.S. Rao, P.L. Xie, X. Cao, T. Rao, et al., Harmine enhances type H vessel formation and prevents bone loss in ovariectomized mice, Theranostics 8 (9) (2018) 2435–2446, https://doi.org/10.7150/thno.22144.

[20] S. Caruso, I.K.H. Poon, Apoptotic cell-derived extracellular vesicles: more than just debris, Front. Immunol. 9 (2018) 1486, https://doi.org/10.3389/fimmu.2018.01486.

[21] E.I. Buzas, B. Gyorgy, G. Nagy, A. Falus, S. Gay, Emerging role of extracellular vesicles in inflammatory diseases, Nat. Rev. Rheumatol. 10 (6) (2014) 356–364, https://doi.org/10.1038/nrrheum.2014.19.

[22] D. Liu, X. Kou, C. Chen, S. Liu, Y. Liu, W. Yu, et al., Circulating apoptotic bodies maintain mesenchymal stem cell homeostasis and ameliorate osteopenia via transferring multiple cellular factors, Cell Res. 28 (9) (2018) 918–933, https://doi.org/10.1038/s41422-018-0070-2.

[23] J. Savill, I. Dransfield, C. Gregory, C. Haslett, A blast from the past: clearance of apoptotic cells regulates immune responses, Nat. Rev. Immunol. 2 (12) (2002) 965–975, https://doi.org/10.1038/nri957.

[24] S. Cenci, M.N. Weitzmann, C. Roggia, N. Namba, D. Novack, J. Woodring, et al., Estrogen deficiency induces bone loss by enhancing T-cell production of TNF-alpha, J. Clin. Invest. 106 (10) (2000) 1229–1237, https://doi.org/10.1172/JCI11066.

[25] H. Liu, S. Liu, X. Qiu, X. Yang, L. Bao, F. Pu, et al., Donor MSCs release apoptotic bodies to improve myocardial infarction via autophagy regulation in recipient cells, Autophagy (2020) 1–16, https://doi.org/10.1080/15548627.2020.1717128.

[26] B. Bussolati, G. Camussi, Renal injury: early apoptotic extracellular vesicles in injury and repair, Nat. Rev. Nephrol. 13 (9) (2017) 523–524, https://doi.org/10.1038/nrneph.2017.117.

[27] C. Penaloza, L. Lin, R.A. Lockshin, Z. Zakeri, Cell death in development: shaping the embryo, Histochem. Cell Biol. 126 (2) (2006) 149–158, https://doi.org/10.1007/s00418-006-0214-1.

[28] K.E. Ensrud, C.J. Crandall, Osteoporosis. Ann Intern Med. 167 (3) (2017) ITC17–ITC32, https://doi.org/10.7326/AITC201708010.

[29] J. Zhu, P.F. Petit, B.J. Van den Eynde, Apoptosis of tumor-infiltrating T lymphocytes: a new immune checkpoint mechanism, Cancer Immunol. Immunother. 68 (5) (2019) 835–847, https://doi.org/10.1007/s00262-018-2269-y.

[30] S. Nagata, P. Golstein, The Fas death factor, Science 267 (5203) (1995) 1449–1456, https://doi.org/10.1126/science.7533326.

[31] M. Romano, G. Fanelli, C.J. Albany, G. Giganti, G. Lombardi, Past, present, and future of regulatory T cell therapy in transplantation and autoimmunity, Front. Immunol. 10 (2019) 43, https://doi.org/10.3389/fimmu.2019.00043.

[32] M.D. Carcao, Side-effects and venous access issues with immune tolerance therapy, Haemophilia 15 (2) (2009) 494–500, https://doi.org/10.1111/j.1365-2516.2008.01951.x.

[33] J. Bae, J.W. Park, Preparation of an injectable depot system for long-term delivery of alendronate and evaluation of its anti-osteoporotic effect in an ovariectomized rat model, Int. J. Pharm. 480 (1–2) (2015) 37–47, https://doi.org/10.1016/j.ijpharm.2015.01.020.

[34] L. Huang, X. Wang, H. Cao, L. Li, D.H. Chow, L. Tian, et al., A bone-targeting delivery system carrying osteogenic phytomolecule icaritin prevents osteoporosis in mice, Biomaterials 182 (2018) 58–71, https://doi.org/10.1016/j.biomaterials.2018.07.046.

[35] J. Wu, D.H. Bremner, S. Niu, D. Li, R. Tang, L.M. Zhu, Multifunctional A7R peptide-modified hollow mesoporous silica@Ag(2)S nanotheranostics for photoacoustic/near-infrared fluorescence imaging-guided tumor-targeted chemo-photothermal therapy, J. Biomed. Nanotechnol. 15 (7) (2019) 1415–1431, https://doi.org/10.1166/jbn.2019.2729.

[36] J.G. Croissant, Y. Fatieiev, A. Almalik, N.M. Khashab, Mesoporous silica and organosilica nanoparticles: physical chemistry, biosafety, delivery strategies, and biomedical applications, Adv Healthc Mater 7 (4) (2018), https://doi.org/10.1002/adhm.201700831.

[37] H. Kuang, S. Yang, Y. Wang, Y. He, K. Ye, J. Hu, et al., Electrospun bilayer composite vascular graft with an inner layer modified by polyethylene glycol and haparin to regenerate the blood vessel, J. Biomed. Nanotechnol. 15 (1) (2019) 77–84, https://doi.org/10.1166/jbn.2019.2666.

[38] S. Elmore, Apoptosis: a review of programmed cell death, Toxicol. Pathol. 35 (4) (2007) 495–516, https://doi.org/10.1080/01926230701320337.

[39] I.K. Poon, C.D. Lucas, A.G. Rossi, K.S. Ravichandran, Apoptotic cell clearance: basic biology and therapeutic potential, Nat. Rev. Immunol. 14 (3) (2014) 166–180, https://doi.org/10.1038/nri3607.

[40] H.D. Ryoo, A. Bergmann, The role of apoptosis-induced proliferation for regeneration and cancer, Cold Spring Harb Perspect Biol 4 (8) (2012) a008797, https://doi.org/10.1101/cshperspect.a008797.

[41] A. Galleu, Y. Riffo-Vasquez, C. Trento, C. Lomas, L. Dolcetti, T.S. Cheung, et al., Apoptosis in mesenchymal stromal cells induces in vivo recipient-mediated immunomodulation, Sci. Transl. Med. 9 (416) (2017), https://doi.org/10.1126/scitranslmed.aam7828.

[42] G.K. Atkin-Smith, R. Tixeira, S. Paone, S. Mathivanan, C. Collins, M. Liem, et al., A novel mechanism of generating extracellular vesicles during apoptosis via a beads-on-a-string membrane structure, Nat. Commun. 6 (2015) 7439, https://doi.org/10.1038/ncomms8439.